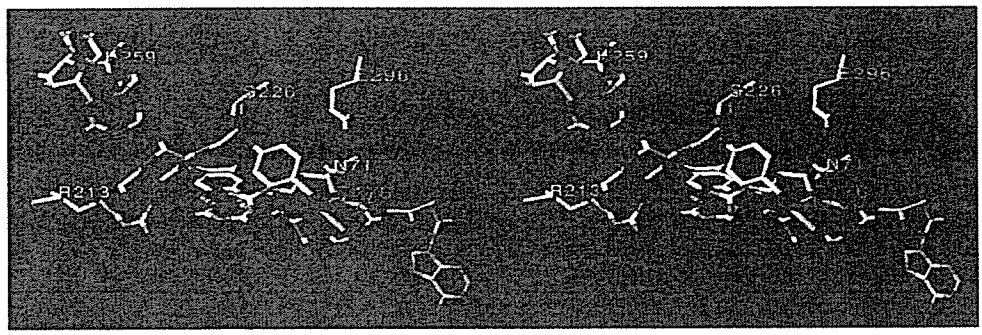

FIGURE 9. **Essential residues in the active site of *S. aureus* MurB.** Essential residues and FAD were mapped on the x-ray structure of *S. aureus* MurB, which was superimposed with the structure of UDP-GlcNAcEP that was obtained from the structure of the *E. coli* MurB-UDP-GlcNAcEP complex.

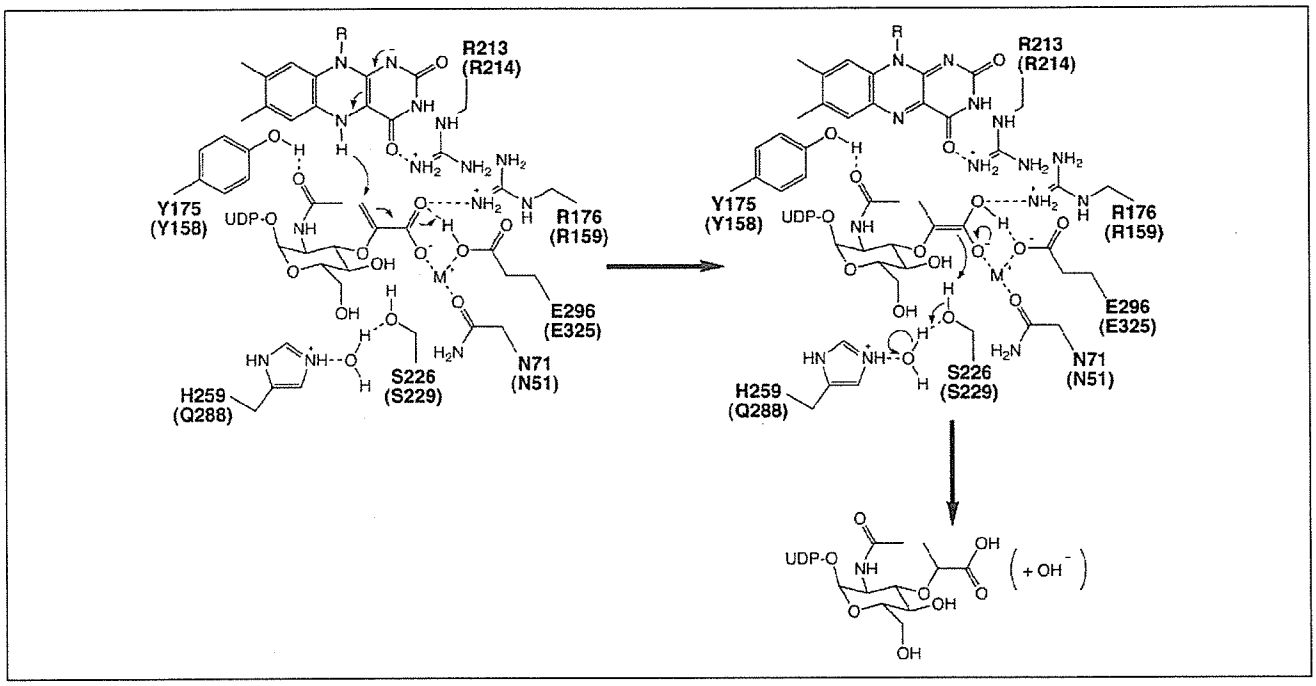

FIGURE 10. **Schematic representation of the second half of the reaction mediated by MurB.** Shown are the interactions of FAD or substrate UDP-GlcNAcEP with essential residues of MurB as determined in this study. The *number in parentheses* represents the amino acid residue of *E. coli* MurB. Predicted hydrogen bonds are indicated by *dotted lines*. M^+ indicates the location of the cationic ion based on a previous report (13) and assumes the presence of a water molecule.

is essential for the UDP-GlcNAcEP reducing activity of MurB. This finding is consistent with suggestion that the side-chain guanidinium of Arg^{213} makes a hydrogen bond with the isoalloxazine ring of FAD (12, 13) (Figs. 9 and 10). Alternatively, the loss of the interaction between Arg^{213} and the isoalloxazine ring of FAD might change the intramolecular location of FAD in MurB, which makes hydride transfer from $FADH_2$ to the enolpyruvyl moiety of UDP-GlcNAcEP impossible.

The second category includes R176A, for which the inhibitory effect of UDP-GlcNAcEP on NADPH oxidation was greatly reduced and whose interaction with UDP-GlcNAcEP could not be detected by difference spectrum analysis. These results suggest that Arg^{176} plays an important role in the binding of the substrate, UDP-GlcNAcEP. It should be emphasized that Arg^{176} is critical for interaction with UDP-GlcNAcEP but not with $NADP^+$, although the two ligands are thought to share the same binding pocket. X-ray structural analysis of *E. coli* MurB revealed that the side-chain guanidinium of Arg^{159}, which corresponds to Arg^{176} in *S. aureus* MurB, forms a hydrogen bond with the substrate's enolpyruvyl moiety. This interaction is thought to contribute to the formation and stabilization of the reaction intermediate (13) (Figs. 9 and 10). Therefore, the inability to make this hydrogen bond in R176A might explain its loss of affinity for and ability to reduce UDP-GlcNAcEP.

The third category includes H259A. Difference spectrum analyses of H259A showed an abnormality in the interaction with both UDP-GlcNAcEP and $NADP^+$. In addition, H259A diminished the inhibitory effect of UDP-GlcNAcEP on NADPH oxidation under aerobic conditions. Thus, it appears that His^{259} is important for interaction with both UDP-GlcNAcEP and $NADP^+$. This is consistent with the previous idea that UDP-GlcNAcEP and $NADP^+$ share the same binding pocket on MurB. These results are the first to identify residues that are crucial for the interaction of MurB and its two substrates, UDP-GlcNAcEP and $NADP^+$. His^{259} of *S. aureus* MurB corresponds to Gln^{288} of *E. coli* MurB, which forms a hydrogen bond with a water molecule in the active site. This water, in turn, interacts with the catalytic Ser^{229} of *E. coli*

MurB (Ser^{226} in *S. aureus* MurB) and provides it with a proton after it donates a proton to the enolpyruvyl moiety of the substrate during the second half of the reaction (13, 17) (Fig. 10). Thus, it is likely that H259A is unable to reduce UDP-GlcNAcEP due to loss or altered location of this important water molecule.

The fourth category includes N71A, Y175F, S226A, and E296A, which appear to retain the affinity for both $NADP^+$ and UDP-GlcNAcEP because difference spectrum analyses show that the K_d values for each ligand do not differ much from the wild-type values. These four mutant MurB proteins were able to carry out the first step of the MurB reaction because they had the ability to oxidize NADPH and mediate NADPH-dependent intramolecular reduction of FAD to $FADH_2$. However, although the mutated proteins could bind UDP-GlcNAcEP, they could not reduce it. The hydroxyl group of Ser^{226} is thought to transfer a proton to reduce UDP-GlcNAcEP (17, 18). Our finding that *S. aureus* S226A MurB loses the activity to reduce UDP-GlcNAcEP without a severe effect on the substrate interaction is similar to the effects of the S229A mutation on *E. coli* MurB and suggests that these two residues play the same role in MurB (Fig. 10).

The side-chain oxygen of Asn^{71} has been shown to make a hydrogen bond with a water molecule that is critically involved in stabilization of the reaction intermediate during proton transfer from $FADH_2$ (13) (Fig. 10). Therefore, the defect in the second half-reaction in N71A might be due to dislocation of the water molecule. This agrees with previous structural analysis of *E. coli* S226A (17), which also loses an active site water molecule that is critical for supporting the protonation of the enolpyruvyl moiety of UDP-GlcNAcEP. Also, x-ray structural analysis suggested that the main-chain nitrogen of Asn^{71} of *S. aureus* MurB makes a hydrogen bond with the α-phosphate of FAD (12). Our finding that N71A contains a stoichiometric amount of FAD and has an absorption spectrum that is indistinguishable from the wild-type enzyme can be explained by the presence of a hydrogen bond between the main-chain nitrogen of the substituted alanine residue and the α-phosphate of FAD.

Structural analysis has suggested that the proton from the protonated state of the side-chain carboxyl group of Glu^{296} is transferred to the enolpyruvyl group of UDP-GlcNAcEP and stabilizes the intermediate (13) (Fig. 10). Indeed, side-chain carboxyl groups of glutamate or aspartate residues are known to contribute to proton transfer during reducing reactions (*e.g.* Glu^{376} in human medium chain acyl-CoA dehydrogenase (26), Glu^{367} in *Megasphaera elsdenii* short-chain acyl-CoA dehydrogenase (27), Glu^{370} in human glutaryl-CoA dehydrogenase (28), and Asp^{170} in *Penicillium simplissiomun* vanillyl-alcohol oxidase (29). Our present data indicating that E296A loses the ability to reduce UDP-GlcNAcEP without a loss of affinity for the substrate support the idea that Glu^{296} plays a role in the second half of the reaction in which MurB transfers a proton to the substrate (Fig. 10). In the structural model shown in Fig. 9, the side-chain carboxyl group of Glu^{296} faces the opposite direction as the substrate, UDP-GlcNAcEP. This is due to the construction of this structural model using data for the UDP-GlcNAcEP-free form of *S. aureus* MurB. The carboxyl group of Glu^{296} might change its position to UDP-GlcNAcEP upon substrate binding. In fact, a flexible conformation of MurB and dynamic changes upon substrate binding, especially in the substrate binding domain, have been suggested by both x-ray and NMR analyses (12, 15, 16).

Structural analysis has shown that Tyr^{175} of *S. aureus* MurB forms a hydrogen bond with the *N*-acetyl moiety of UDP-GlcNAcEP (12, 13) (Figs. 9 and 10). Thus, our present results, in which Y175F lost the ability to reduce UDP-GlcNAcEP, suggest that the hydrogen bond between Tyr^{175} and the *N*-acetyl moiety of the substrate is important for the suitable positioning of the enolpyruvyl moiety so that the proton can be transferred from $FADH_2$. Structural analysis of the crystal of the Y175F·UDP-GlcNAcEP complex is needed to verify this prediction.

Conclusion—Here, we selected 11 residues that are possibly essential for *S. aureus* MurB activity. These residues were selected because sequence alignment showed they are highly conserved in other bacterial MurB proteins and because x-ray structural analyses have shown that they interact with the substrate UDP-GlcNAcEP or the cofactor FAD. In the present study, each residue was replaced with alanine or phenylalanine, and the resulting mutant genes were examined for their ability to complement the temperature-sensitive growth of a *murB* mutant of *S. aureus*. Seven of the 11 mutated proteins were found to be essential for *in vivo* activity and were further purified and biochemically characterized. These studies identified six residues that are essential for *S. aureus* MurB both *in vivo* and *in vitro*: Asn^{71}, Tyr^{175}, Arg^{176}, Arg^{213}, His^{259}, and Glu^{296}, in addition to Ser^{226}, which was previously reported as essential for the activity of *E. coli* MurB. The results described here support the molecular reaction mechanism predicted by x-ray structure analyses (Fig. 10). This study also identified amino acid residues crucial for the interaction with $NADP^+$ and UDP-GlcNAcEP and further classified them into four categories; the first has a defect in the FAD-bound state, the second has a defect in UDP-GlcNAcEP binding, the third has a defect in the interaction with both UDP-GlcNAcEP and $NADP^+$, and the last is essential for catalysis of the second half of the reaction but does not affect the interactions with substrates. Because MurB is an attractive target for antibiotics, the enzymological data obtained here is expected to contribute to development of antibacterial drugs.

Acknowledgments—We thank Dr. Tomofumi Santa (University of Tokyo) for helpful discussion about HPLC analysis and Drs. Takashi Yutsudo and Kazuhisa Murakami (Shionogi Co. Ltd.) for the supply of purified UDP-GlcNAcEP and UDP-N-acetylmuramic acid. We also thank Naoki Ito, Hiromi Komaki, and Kozue Saito for technical assistance and Hiroshi Kasuga for help in an initial part of this work.

REFERENCES

1. van Heijenoort, J. (1996) in *Escherichia coli and Salmonella: Cellular and Molecular Biology* (Neidhardt, F. C., Curtiss III, R., Ingraham, J. L., Lin, E. C. C., Low, K. B., Magasanik, B., Reznikoff, W. S., Riley, M., Schaechter, M., and Umbarger, H. E., eds) 2nd Ed., pp. 1025–1034, American Society for Microbiology, Washington, D. C.
2. Holtje, J. V. (1998) *Microbiol. Mol. Biol. Rev.* **62**, 181–203
3. Navarre, W. W., and Schneewind, O. (1999) *Microbiol. Mol. Biol. Rev.* **63**, 174–229
4. Miyakawa, T., Matsuzawa, H., Matsuhashi, M., and Sugino, Y. (1972) *J. Bacteriol.* **112**, 950–958
5. Rowland, S. L., Errington, J., and Wake, R. G. (1995) *Gene (Amst.)* **164**, 113–116
6. Matsuo, M., Kurokawa, K., Nishida, S., Li, Y., Takimura, H., Kaito, C., Fukuhara, N., Maki, H., Miura, K., Murakami, K., and Sekimizu, K. (2003) *FEMS Microbiol. Lett.* **222**, 107–113
7. El Zoeiby, A., Sanschagrin, F., and Levesque, R. C. (2003) *Mol. Microbiol.* **47**, 1–12
8. Gotz, F. (2004) *Curr. Opin. Microbiol.* **7**, 477–487
9. Andres, C. J., Bronson, J. J., D'Andrea, S. V., Deshpande, M. S., Falk, P. J., Grant-Young, K. A., Harte, W. E., Ho, H. T., Misco, P. F., Robertson, J. G., Stock, D., Sun, Y., and Walsh, A. W. (2000) *Bioorg. Med. Chem. Lett.* **10**, 715–717
10. Bronson, J. J., DenBleyker, K. L., Falk, P. J., Mate, R. A., Ho, H. T., Pucci, M. J., and Snyder, L. B. (2003) *Bioorg. Med. Chem. Lett.* **13**, 873–875
11. Murzin, A. G. (1996) *Curr. Opin. Struct. Biol.* **6**, 386–394
12. Benson, T. E., Harris, M. S., Choi, G. H., Cialdella, J. I., Herberg, J. T., Martin, J. P., Jr., and Baldwin, E. T. (2001) *Biochemistry* **40**, 2340–2350
13. Benson, T. E., Filman, D. J., Walsh, C. T., and Hogle, J. M. (1995) *Nat. Struct. Biol.* **2**, 644–653
14. Dhalla, A. M., Yanchunas, J., Jr., Ho, H. T., Falk, P. J., Villafranca, J. J., and Robertson, J. G. (1995) *Biochemistry* **34**, 5390–5402
15. Farmer, B. T., II, Constantine, K. L., Goldfarb, V., Friedrichs, M. S., Wittekind, M., Yanchunas, J., Jr., Robertson, J. G., and Mueller, L. (1996) *Nat. Struct. Biol.* **3**, 995–997
16. Constantine, K. L., Mueller, L., Goldfarb, V., Wittekind, M., Metzler, W. J., Yanchunas, J.,

Jr., Robertson, J. G., Malley, M. F., Friedrichs, M. S., and Farmer, B. T., II (1997) *J. Mol. Biol.* **267,** 1223–1246
17. Benson, T. E., Walsh, C. T., and Hogle, J. M. (1997) *Biochemistry* **36,** 806–811
18. Benson, T. E., Walsh, C. T., and Massey, V. (1997) *Biochemistry* **36,** 796–805
19. Sambrook, J., and Russell, D. W. (2001) *Molecular Cloning: A Laboratory Manual*, 3rd Ed., pp. 13.36–13.39, Cold Spring Harbor Laboratory, Cold Spring Harbor, NY
20. Anwar, R. A., and Vlaovic, M. (1979) *Can. J. Biochem.* **57,** 188–196
21. Englander, S. W., Calhoun, D. B., and Englander, J. J. (1987) *Anal. Biochem.* **161,** 300–306
22. Axley, M. J., Fairman, R., Yanchunas, J., Jr., Villafranca, J. J., and Robertson, J. G. (1997) *Biochemistry* **36,** 812–822
23. Benson, T. E., Marquardt, J. L., Marquardt, A. C., Etzkorn, F. A., and Walsh, C. T. (1993) *Biochemistry* **32,** 2024–2030
24. Fraaije, M. W., Van Berkel, W. J., Benen, J. A., Visser, J., and Mattevi, A. (1998) *Trends Biochem. Sci.* **23,** 206–207
25. Taku, A., Gunetileke, K. G., and Anwar, R. A. (1970) *J. Biol. Chem.* **245,** 5012–5016
26. Bross, P., Engst, S., Strauss, A. W., Kelly, D. P., Rasched, I., and Ghisla, S. (1990) *J. Biol. Chem.* **265,** 7116–7119
27. Becker, D. F., Fuchs, J. A., Banfield, D. K., Funk, W. D., MacGillivray, R. T., and Stankovich, M. T. (1993) *Biochemistry* **32,** 10736–10742
28. Dwyer, T. M., Rao, K. S., Goodman, S. I., and Frerman, F. E. (2000) *Biochemistry* **39,** 11488–11499
29. van den Heuvel, R. H., Fraaije, M. W., Mattevi, A., and van Berkel, W. J. (2000) *J. Biol. Chem.* **275,** 14799–14808

The American Journal of Pathology, Vol. 169, No. 4, October 2006

DOI: 10.2353/ajpath.2006.060034

Cell Injury, Repair, Aging and Apoptosis

Overexpression of Peroxisome Proliferator-Activated Receptor γ Co-Activator-1α Leads to Muscle Atrophy with Depletion of ATP

Shinji Miura,* Eriko Tomitsuka,† Yasutomi Kamei,*‡ Tomomi Yamazaki,* Yuko Kai,* Mayumi Tamura,* Kiyoshi Kita,† Ichizo Nishino,§ and Osamu Ezaki*

From the Nutritional Science Program, National Institute of Health and Nutrition, Tokyo; the Department of Biomedical Chemistry,† Graduate School of Medicine, The University of Tokyo, Tokyo; the Department of Molecular Medicine and Metabolism,‡ Medical Research Institute, Tokyo Medical and Dental University, Tokyo; and the Department of Neuromuscular Research,§ National Institute of Neuroscience, National Center of Neurology and Psychiatry, Tokyo, Japan*

Peroxisome proliferator-activated receptor-γ co-activator-1α (PGC-1α) is a key nuclear receptor co-activator for mitochondrial biogenesis. Here we report that overexpression of PGC-1α in skeletal muscles increased mitochondrial number and caused atrophy of skeletal muscle, especially type 2B fiber-rich muscles (gastrocnemius, quadriceps, and plantaris). Muscle atrophy became evident at 25 weeks of age, and a portion of the muscle was replaced by adipocytes. Mice showed increased energy expenditure and reduced body weight; thyroid hormone levels were normal. Mitochondria exhibited normal respiratory chain activity per mitochondrion; however, mitochondrial respiration was not inhibited by an ATP synthase inhibitor, oligomycin, clearly indicating that oxidative phosphorylation was uncoupled. Accordingly, ATP content in gastrocnemius was markedly reduced. A similar phenotype is observed in Luft's disease, a mitochondrial disorder that involves increased uncoupling of respiration and muscle atrophy. Our results indicate that overexpression of PGC-1α in skeletal muscle increases not only mitochondrial biogenesis but also uncoupling of respiration, resulting in muscle atrophy. ***(Am J Pathol 2006, 169:1129–1139; DOI: 10.2353/ajpath.2006.060034)***

Peroxisome proliferator-activated receptor (PPAR)-γ co-activator-1α (PGC-1α), which was identified as co-activator of nuclear receptors, is expressed in brown adipose tissue, skeletal muscle, heart, kidney, and brain and is markedly up-regulated in brown adipose tissue and skeletal muscle after acute exposure to cold stress.[1] Increased expression of PGC-1α as part of activated adaptive thermogenesis occurs primarily in the mitochondria of brown adipose tissue and skeletal muscle through stimulation of mitochondrial biogenesis and respiration.[2] PGC-1α is also believed to be a key molecule involved in fatty acid oxidation because it was found to interact with PPARα to promote transcription of nuclear genes encoding mitochondrial fatty acid oxidation enzymes.[3,4] In *in vivo* studies of muscles overexpressing PGC-1α, the skeletal muscles showed a red color characteristic of oxidative muscle and elevated levels of enzymes related to mitochondrial oxidative phosphorylation and fatty acid oxidation.[5] These same muscles showed reduced GLUT4 mRNA expression and impaired insulin tolerance.[6] In brown adipose tissue mitochondria, as observed during prolonged exposure to cold, PGC-1α promotes uncoupling of respiration through induction of uncoupling protein 1 (UCP1).[1] When respiration is uncoupled, the membrane potential energy is channeled to heat production rather than to adenosine triphosphate (ATP) production, which may cause functional abnormalities and cell death. In C2C12 myocytes, increased uncoupling of respiration driven by PGC-1α was observed.[7] Overexpression of PGC-1α promoted mitochondrial biogenesis and resulted in dilated cardiomyopathy.[4] These data suggest that PGC-1α overexpression in skeletal muscles increases uncoupling of respiration, decreases

Supported in part by the Japanese Ministry of Education, Culture, Sports, Science, and Technology (MEXT, Tokyo) (grant-in-aid for scientific research (KAKENHI) and the 21st Century COE Program); the Japanese Ministry of Health, Labor, and Welfare (Tokyo); and the Promotion of Fundamental Studies in Health Sciences of the National Institute of Biomedical Innovation (NIBIO).

Accepted for publication June 27, 2006.

Address reprint requests to Shinji Miura, Ph.D., or Osamu Ezaki, M.D., Nutritional Science Program, National Institute of Health and Nutrition, 1-23-1, Toyama, Shinjuku-ku, Tokyo 162-8636, Japan. E-mail: shinjim@nih.go.jp and ezaki@nih.go.jp.

ATP content, and results in muscle atrophy. However, this hypothesis has not been verified. In the present study, we examined mitochondrial respiratory function and morphological changes in the skeletal muscles of mice overexpressing PGC-1α and found that PGC-1α transgenic mice had markedly decreased ATP content in skeletal muscles and developed myopathy at 25 weeks of age, which recapitulates the phenotype of Luft's disease.[8–10]

Materials and Methods

Animals and Treatments

D-line mice expressed 10-fold higher PGC-1α mRNA and E-line mice expressed 13-fold higher PGC-1α mRNA in skeletal muscle compared to wild-type mice, as described in our previous study.[6] Male chimeras harboring the PGC-1 transgene were mated with pure C57BL/6J females (Tokyo Laboratory Animals Science, Tokyo, Japan) to obtain F_1 offspring. The heterozygous F_1 male offspring from this breeding were then backcrossed with purebred C57BL/6J females to obtain F_2 offspring, and this process was continued until the F_3 generation of mice was obtained. Heterozygous transgenic mice were used for the following studies.

Mice were fed a standard laboratory chow diet (CE2; Clea, Tokyo, Japan). Mice were exposed to a 12-hour light/dark cycle and maintained at a constant temperature of 22°C. The mice were cared for in accordance with "Principles of Laboratory Animal Care" (National Institutes of Health publication no. 85-23, revised 1985: *http://grants1.nih.gov/grants/olaw/references/phspol.htm*) and our institutional guidelines.

Oxygen consumption was measured with a metabolic chamber as described previously.[11] For estimation of running wheel activity, mice were housed individually in cages (9 × 22 × 9 cm) equipped with a running wheel (20-cm diameter; Shinano Co., Tokyo, Japan). Each wheel revolution was registered by a magnetic switch connected to a counter. The number of revolutions was recorded daily for 10 days.

Histological Analyses

Samples of the tibialis anterior muscle at 16 weeks of age and hindlimb at 25 weeks of age were frozen in liquid nitrogen-cooled isopentane, and transverse serial sections were stained with hematoxylin and eosin (H&E), modified Gomori trichrome, and Oil red O.[12] These sections were also analyzed by enzyme histochemistry to evaluate cytochrome *c* oxidase (COX)[13] and succinate dehydrogenase (SDH) activities.[14] For electron microscopy, extensor digitorum longus muscles from 16-week-old mice were fixed in buffered 2% isotonic glutaraldehyde (pH 7.4), postfixed in osmium tetroxide, and embedded in epoxy resin. Ultrathin sections were stained with uranyl acetate and lead nitrate and examined with an H-7000 electron microscope (Hitachi, Tokyo, Japan).

Preparation of the Mitochondrial Fraction from Skeletal Muscle

Skeletal muscles (gastrocnemius and quadriceps) from both 14-week-old wild-type and PGC-1α transgenic male mice were pooled from three mice in each group. Tissues were cut with scalpels and treated with 1 ml of protease buffer containing 0.1 mol/L KCl, 50 mmol/L Tris-HCl (pH 7.5), 5 mmol/L $MgSO_4$, 1 mmol/L ethylenediaminetetraacetic acid (EDTA), 5 mg/ml bovine serum albumin, 1 mmol/L ATP, and 2 mg/ml proteinase K for 2 minutes on ice. Tissues were then washed with ATP buffer containing 0.1 mol/L KCl, 50 mmol/L Tris-HCl (pH 7.5), 5 mmol/L $MgSO_4$, 1 mmol/L EDTA, 5 mg/ml bovine serum albumin, and 1 mmol/L ATP. The washed tissues were homogenized in 10 ml of ATP buffer with a glass/Teflon homogenizer in a power-driven Potter-Elvehjem homogenizer (Kadoguchi-Keiki, Tokyo, Japan). The homogenate was brought to 15 ml and centrifuged at 600 × *g* for 10 minutes to remove cell debris and nuclei. The supernatant was then centrifuged at 4500 × *g* for 15 minutes. The pellet was washed with KCl buffer containing 0.1 mol/L KCl, 50 mmol/L Tris-HCl (pH 7.5), 5 mmol/L $MgSO_4$, 1 mmol/L EDTA, and 5 mg/ml bovine serum albumin and centrifuged at 7000 × *g* for 15 minutes. The mitochondrial pellet was resuspended in mitochondrial buffer containing 225 mmol/L mannitol and 75 mmol/L sucrose.[15] Protein concentrations were estimated by Lowry method.[16]

Measurement of Mitochondrial Respiration

Mitochondrial respiration was measured with Biological Oxygen Monitor 5300 (Yellow Springs Instrument, Yellow Springs, OH) was performed using Clark-type oxygen electrodes.[17] Respiration buffer containing 225 mmol/L mannitol, 75 mmol/L sucrose, 10 mmol/L Tris-HCl (pH 7.2), 5 mmol/L potassium phosphate (pH 7.2), and 10 mmol/L KCl was used. Five mmol/L succinate as substrate and 100 μg of mitochondria and 5 μg/ml rotenone were added, and respiration was started by the addition of 5 mmol/L potassium succinate. State 3 respiration was started by the addition of 200 μmol/L ADP (Sigma, St. Louis, MO). Finally, 2.5 μg/ml oligomycin (Sigma) was added as an inhibitor of ATP synthetase to block all phosphorylation-related respiration.[2]

Enzymatic Activity of the Respiratory Complex

SDH activity was measured by monitoring the change in absorbance 3-(4,5-dimethylthiazol-2-yl)-2,5-diphenyl-2,4-tetrazolium bromide (MTT) at 570 nm in the presence of phenazine methosulfate with the 17 $mmol/L^{-1}cm^{-1}$ extinction coefficient for MTT.[18] Succinate-ubiquinone oxidoreductase activity was measured in the presence of 2,3–2,6-dichlorophenolindophenol (DCIP) with the 21 $mmol/L^{-1}cm^{-1}$ extinction coefficient for DCIP.[18] NADH-ubiquinone reductase activity was assayed in 50 mmol/L potassium phosphate buffer (pH 7.7), 200 μmol/L NADH, 2 mmol/L KCN, and 90 μmol/L ubiquinone-1. Oxidation of NADH was monitored at 340 nm with a $mmol/L^{-1}$ extinc-

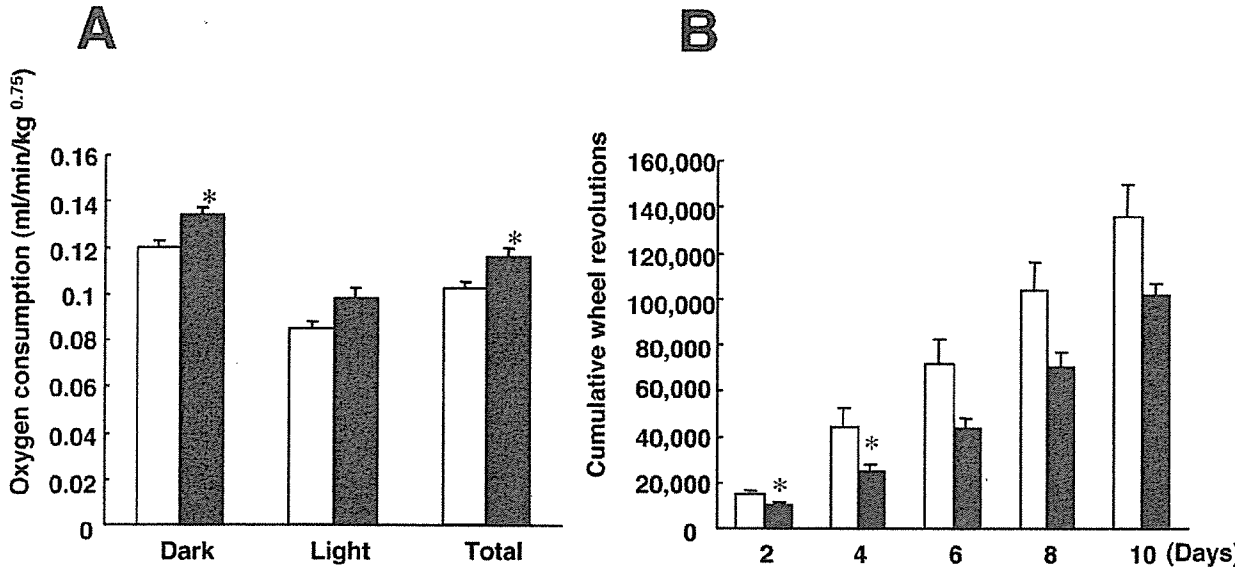

Figure 1. PGC-1α overexpression increases energy expenditure. **A:** Oxygen consumption in PGC-1α mice. Oxygen consumption by 10-week-old female mice housed individually was monitored during the dark cycle (7 p.m. to 7 a.m.) and the light cycle (7 a.m. to 7 p.m.). Each column shows the mean ± SEM values. Open column, wild type; closed column, PGC-1α mice. Wild type, $n = 3$; PGC-1α mice, $n = 6$ (a mixture of three D-line and three E-line mice). $^*P < 0.05$ versus wild-type mice. **B:** Running wheel activities of PGC-1α mice. The number of revolutions was recorded daily for 10 days, and cumulative values are shown. Open column, wild type; closed column, PGC-1α mice. Mice were 8-week-old females. Wild type, $n = 3$; PGC-1α mice, $n = 6$ (a mixture of three D-line and three E-line mice). $^*P < 0.05$ versus wild-type mice.

tion coefficient of 6.2 for NADH.[19] NADH oxidase activity was assayed in 50 mmol/L potassium phosphate buffer (pH 7.7) and 200 μmol/L NADH in the presence or absence of 100 nmol/L antimycin A and 2 mmol/L KCN. The oxidation of NADH was monitored at 340 nm with a mmol/L^{-1} extinction coefficient of 6.2 for NADH.[20] NADH-cytochrome *c* reductase, succinate-cytochrome *c* reductase, ubiquinol-cytochrome *c* reductase, and COX activities were measured as described previously.[17,21] Citrate synthase activity was measured as described previously.[22] Each measurement was performed in three times.

Northern Blot Analysis

Northern blot analysis was performed as described previously.[23]

Southern Blot Analysis

To measure mitochondrial DNA (mtDNA) copy number, cDNA probes for mtDNA-COX II and nuclear genome gene-COX IV were generated as described previously.[6] For each sample, 10 μg of total DNA (containing both genomic and mitochondrial DNAs) from gastrocnemius were digested with *Eco*RI and *Nco*I, separated by electrophoresis on 0.8% agarose gels, and transferred overnight to nylon membranes.[1] Blots were then hybridized to COX II and COX IV probes radiolabeled with ^{32}P-dCTP. The blots were washed, and DNA were quantified with an image analyzer (BAS 1800; Fuji Film, Tokyo, Japan) and expressed as the intensity of phosphostimulated luminescence.

Real-Time Polymerase Chain Reaction (PCR) Analysis

Reactions were performed in the 96-well format with SYBR Green PCR Master Mix and a 7500 real-time PCR system (Applied Biosystems, Foster City, CA) with 3 ng of total genomic DNA as template. As a preliminary experiment, we determined appropriate amounts of DNA for the assay. Copy number of COX II was normalized to those of COX IV and 36B4. 36B4 encodes acidic ribosomal phosphoprotein PO,[24] and the 36B4 cDNA probe is widely used as a control in RNase protection experiments to study regulation of the transcription of several genes by estradiol. Mouse-specific primer pairs were: COX II forward, 5′-CCGACTAAATCAAGCAACAGTAACA-3′ and COX II reverse, 5′-AAATTTCAGAGCATTGGCCATAG-3′; COX IV forward, 5′-CTATGTGTATGGCCCCATCC-3′ and COX IV reverse, 5′-AGCGGGCTCTCACTTCTTC-3′; and 36B4 forward, 5′-GGCCCTGCACTCTCGCTTTC-3′ and 36B4 reverse, 5′-TGCCAGGACGCGCTTGT-3′.

Measurement of mtDNA Copy Number

The mtDNA content is the mtDNA copy number normalized to the copy number of a gene contained in the nuclear genome. The mtDNA copy number in PGC-1α transgenic mice was expressed by percentages of those in control wild-type mice with the formula: [(mtDNA in PGC-1α transgenic mice/nuclear genome gene in PGC-1α transgenic mice)/(mtDNA in wild-type mice/nuclear genome gene in wild-type mice)] × 100%. Southern

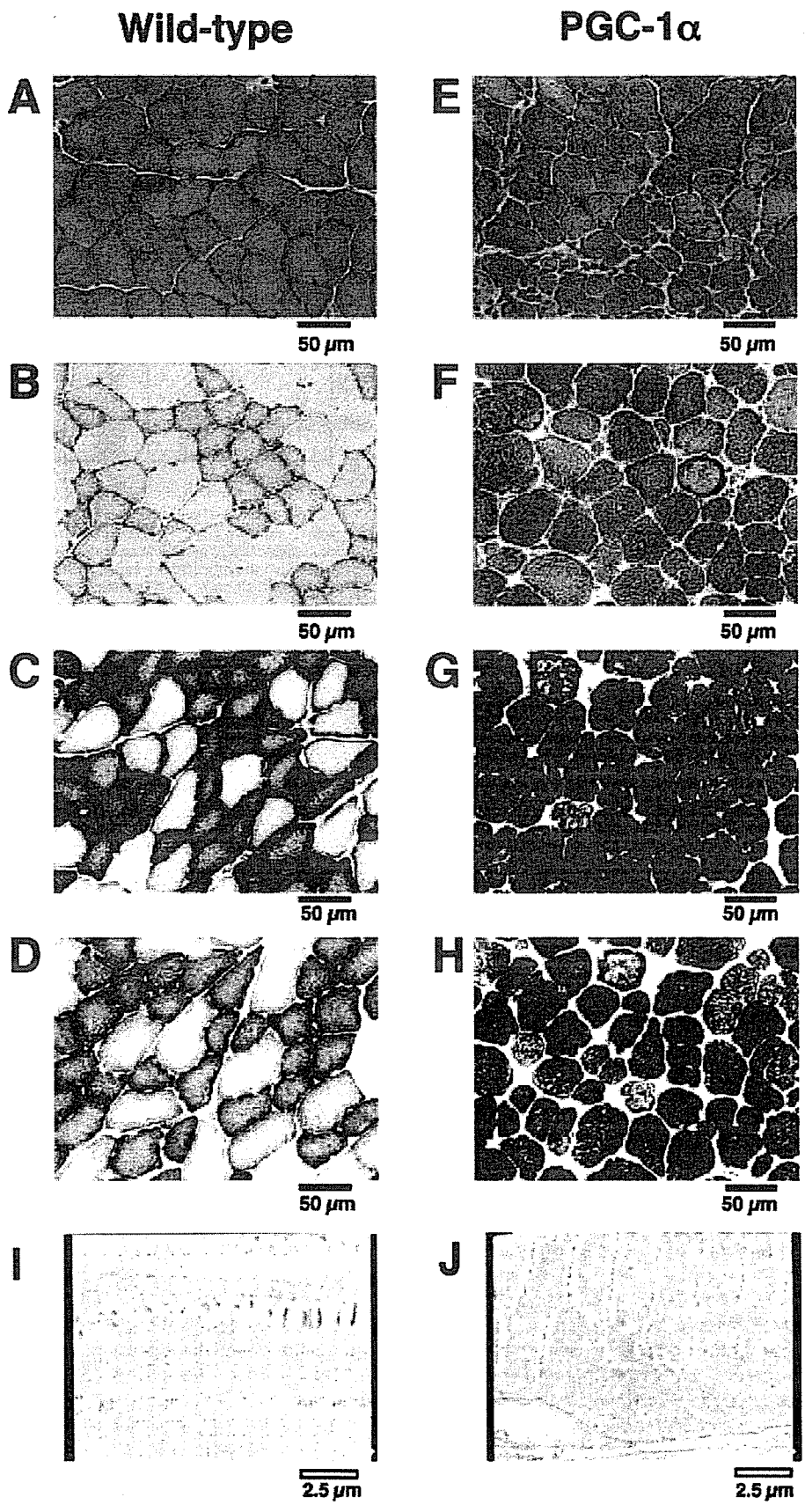
Wild-type
PGC-1α
A
E
50 μm
B
F
50 μm
C
G
50 μm
D
H
50 μm
I
J
2.5 μm
2.5 μm

blotting and real-time PCR were used to estimate the copy number of specific genes in skeletal muscles. The mitochondrial gene used for mtDNA copy estimation was COX II, and the copy number of COX II was normalized to the copy number of one of two genes, COX IV or 36B4, contained in the nuclear genome.

Measurements of ATP and AMP Contents

Gastrocnemius was homogenized with 1.0 N perchloric acid and centrifuged at 10,000 × *g* for 15 minutes. After neutralization of the supernatant with calcium carbonate, ATP and AMP concentrations were determined by high performance liquid chromatogram (Phenomenex Luna 5 μ NH_2; mobile phase, sodium phosphate buffer; detector, 260 nm; Torrance, CA).[25,26]

Body Composition Analysis

Mice were anesthetized with pentobarbital sodium, Nembutal (0.08 mg/g body weight; Abbot Laboratories, Chicago, IL), and scanned with a Lunar PIXI mus2 densitometer (Lunar Corp., Madison, WI), equipped for dual-energy X-ray absorptiometry (DEXA).[27]

Statistical Analysis

All data are presented as mean ± SEM. Data from multiple groups were compared by one-way analysis of variance (StatView 5.0; Abacus Concepts, Berkeley, CA). When differences were significant, data were compared between groups by Fisher's protected least significant difference test. Data from two experimental groups were compared by unpaired Student's *t*-test. Statistical significance was defined as $P < 0.05$.

Results

PGC-1α Transgenic Mice Show Increased Energy Expenditure

In our previous study, skeletal muscles of PGC-1α transgenic mice showed the red color characteristic of oxidative muscle and increased levels of enzymes related to mitochondrial oxidative phosphorylation. In the same mice, expression of GLUT4 mRNA was reduced, and the glucose-lowering effects of insulin were impaired.[6] To determine whether PGC-1α transgenic mice show increased energy expenditure, whole-body oxygen consumption was measured in 10-week-old mice (Figure 1A). During both the dark (active) and light (sleeping) phases, PGC-1α transgenic mice showed 1.1-fold higher oxygen consumption than control mice. Because the cumulative number of wheel revolutions was 20% less in PGC-1α transgenic mice (Figure 1B), the increased oxygen consumption in PGC-1α transgenic mice was not attributable to increased voluntary exercise.

Blood triiodothyronine (T3) and thyroxine (T4) concentrations were not altered in 10-week-old PGC-1α transgenic mice. Blood T3 concentrations in wild-type mice, D-line transgenic mice, and E-line transgenic mice were 1.16 ± 0.07 ng/ml, 1.14 ± 0.04 ng/ml, and 1.06 ± 0.01 ng/ml (n = 3 each group), respectively. Blood T4 concentrations in wild-type mice, D-line transgenic mice, and E-line transgenic mice were 5.89 ± 0.63 μg/dl, 5.78 ± 0.58 μg/dl, and 5.55 ± 0.29 μg/dl (n = 3 each group), respectively.

Numbers of Normal-Sized Mitochondria Were Increased in Skeletal Muscles from PGC-1α Transgenic Mice

We examined whether biogenesis of mitochondria and respiratory chain activity were increased in skeletal muscles from PGC-1α transgenic mice using histochemical staining of tibialis anterior muscle (type 2B-rich fiber muscle) in 16-week-old D-line transgenic mice (Figure 2). H&E staining revealed increased variability in muscle fiber size and increased interstitial cell number and connective tissues in PGC-1α transgenic mice (Figure 2E). Modified Gomori trichrome staining revealed a marked increase in the number of mitochondria in PGC-1α transgenic mice (Figure 2F). In addition, increased COX (Figure 2G) and SDH (Figure 2H) activities in transgenic muscle indicated that the mitochondrial respiratory chain was functional and active. The pathological hallmarks of mtDNA disease, such as ragged-red fibers and COX deficiency,[28] were not observed.

To examine the subcellular structure of myocytes in PGC-1α transgenic mice in detail, extensor digitorum longus skeletal muscle in 16-week-old E-line transgenic mice was examined by electron microscopy (Figure 2J). An increase in the thickness of the *Z*-band that is seen in type-1 fibers and a marked increase in the number of mitochondria in the subsarcolemmal region of muscle fibers were observed. Mitochondrial size was normal, and the alignment of myofibrils was intact in transgenic mice.

To estimate numbers of mitochondria in gastrocnemius from PGC-1α transgenic mice, citrate synthase activity, the most commonly used marker of mitochondrial number,[17] and mtDNA (COX II) copy number relative to those

Figure 2. Morphological analysis of skeletal muscles. Tissue sections from tibialis anterior muscle from 16-week-old wild-type (**A–D**) and PGC-1α transgenic (D-line) mice (**E–H**) are presented. **A** and **E:** H&E staining of tibialis anterior muscle. There are scattered atrophic fibers in PGC-1α transgenic muscle. **B** and **F:** Modified Gomori trichrome staining. An increase in the number of mitochondria was observed in PGC-1α transgenic muscle. **C** and **G:** Staining to detect COX activity. **D** and **H:** Staining to detect SDH activity. Activities of these enzymes were greatly increased in myocytes from PGC-1α transgenic mice. Similar results were obtained with E-line transgenic mice (data not shown). **I** and **J:** Electron microscopy of extensor digitorum longus muscles from wild-type control mice (16 weeks of age) (**I**) and PGC-1α transgenic mice (16 weeks of age, E-line) (**J**). Numbers of mitochondria were markedly higher in transgenic mice, especially in the subsarcolemmal region, than in wild-type mice. Similar results were obtained with D-line transgenic mice (data not shown). Scale bars: 50 μm (**A–H**); 2.5 μm (**I, J**).

Table 1. Estimated Numbers of Mitochondria in Gastrocnemius from 14-Week-Old Mice

	Wild type	PGC-1α/D line	PGC-1α/E line
Citrate synthase activity (μmol/minute/mg protein, %)	0.56 (100)	1.75 (313)	1.66 (296)
COX II/COX IV (%, determined by Southern blot)	100 ± 4 (6)	202 ± 21 (3)‡	165 ± 15 (3)†
COX II/COX IV (%, determined by real-time PCR)	100 ± 5 (6)	178 ± 10 (3)†	214 ± 29 (3)‡
COX II/36B4 (%, determined by real-time PCR)	100 ± 5 (6)	203 ± 8 (3)*	292 ± 58 (3)‡

For measurement of citrate synthase activity, tissues from each group were pooled from three animals before mitochondrial isolation, and the citrate synthase activities of pooled samples were measured. For estimation of mtDNA copy number in skeletal muscle, the relative mtDNA copy number in skeletal muscle from individual mice in each group was calculated as the ratio of COX II (mitochondrial) to COX IV or 36B4 (nuclear) genes as determined by Southern blotting and/or real-time PCR. The relative mtDNA copy number was expressed as the percentage of the ratio in wild type. Numbers of mice were indicated. *$P < 0.05$, †$P < 0.01$, and ‡$P < 0.001$ versus wild-type mice.

of nuclear genome genes (COX IV and 36B4), were measured (Table 1). The copy number of COX IV was estimated by two different methods, Southern blotting and real-time PCR. Citrate synthase activity in PGC-1α transgenic mice was threefold higher than that in wild-type mice. The ratio of COX II copy number to genomic DNA copy number in PGC-1α transgenic mice was twofold to threefold higher than that in wild-type mice, regardless of the detection method or nuclear genome reference gene. These data suggested that if we assume no significant differences in citrate synthase activity and mtDNA copy number in mitochondria between PGC-1α transgenic and wild-type mice, the number of mitochondria in gastrocnemius from PGC-1α transgenic mice was twofold to threefold larger than that in wild-type mice.

Increased Uncoupling of Oxidative Phosphorylation in Skeletal Muscle Mitochondria from PGC-1α Transgenic Mice

To study the function of skeletal muscle mitochondria, we compared the respiration rate (=oxygen consumption) in isolated mitochondria from gastrocnemius and quadriceps of PGC-1α transgenic mice with that in wild-type mice in the absence and presence of oligomycin, an inhibitor of the F_1F_0-ATP synthase.[29] First, the respiration rate of mitochondria was measured under conditions in which mitochondrial substrate and ADP were not limiting to mimic state 3 respiration. To measure uncoupled respiration, oligomycin was added to inhibit oxidative phosphorylation before measurement of respiration rates. In the absence of oligomycin, both lines of PGC-1α transgenic mice showed a twofold to threefold increase of respiration rate on a protein basis of mitochondria-rich fraction (Figure 3A). Because the increased respiration rate observed in PGC-1α transgenic mice was likely attributable to an increased mitochondrial number, we divided the respiration rate by the citrate synthase activity to express respiration rate on a per mitochondrion basis.[17] To normalize the respiration rate to the mitochondrial number, citrate synthase activity rather than mtDNA copy number was used, because the same method for preparation of mitochondria was used for both respiration rate and citrate synthase activity assays. When expressed per unit of citrate synthase activity, the respiration rate was similar between PGC-1α transgenic mice and wild-type mice (Figure 3B), suggesting that respiration was comparable in each mitochondrion in PGC-1α

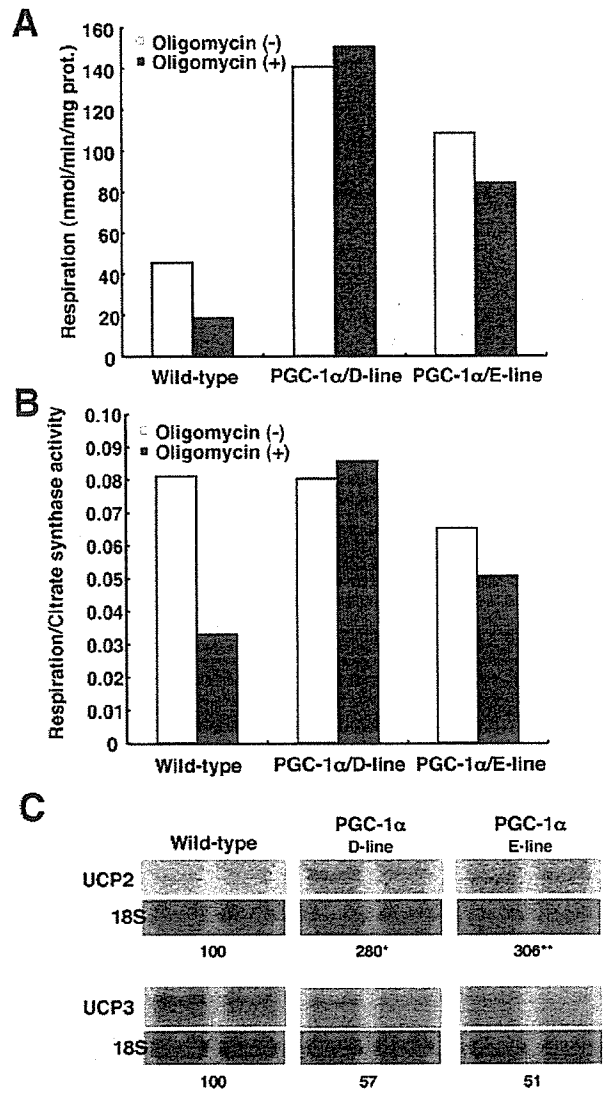

Figure 3. Increased uncoupling of oxidative phosphorylation and UCP2 in skeletal muscle from PGC-1α transgenic mice. Skeletal muscles (gastrocnemius, quadriceps) from both wild-type and PGC-1α male transgenic mice (D-line and E-line) at 14 weeks of age ($n = 3$ each group). Mitochondrial fraction was prepared as described under Materials and Methods. State 3 respiration rate of the mitochondrial fraction was measured in the presence and absence of 2.5 μg/ml oligomycin. Each measurement was performed in triplicate. Each data point is the mean value of the measurements normalized to the protein content (**A**) or to the citrate synthase activity of the fraction (**B**). **C**: Total RNA extracted from gastrocnemius was probed with ^{32}P-labeled human UCP2 and UCP3 cDNA probes. Ribosomal 18S RNA is shown as a loading control. The average densitometric ratios (wild type was set as 100) are under the blot. *$P < 0.05$, **$P < 0.01$ versus wild-type mice.

Table 2. Enzymatic Activity of Respiratory Chain Complexes in Mitochondria from 14-Week-Old Mice

	Enzyme complex (enzyme activity/citrate synthase activity)						
	I	I + III	I + III + IV	II (SDH)	II (SQR)	II + III	IV
Wild type	0.217	0.238	0.279	0.132	0.150	0.177	0.415
PGC-1α/D line	0.201	0.315	0.478	0.102	0.100	0.127	0.868
PGC-1α/E line	0.181	0.225	0.417	0.105	0.099	0.129	0.832

For each group, tissues were pooled from three animals before mitochondrial isolation.

transgenic and wild-type mice. However, the mechanism of respiratory control was different; in wild-type mice, oligomycin-insensitive respiration (=uncoupling) constituted 40% of total respiration, whereas in PGC-1α transgenic mice, most respiration was oligomycin-insensitive. Therefore, PGC-1α transgenic mice contained more mitochondria, but these mitochondria showed lower ATP synthesis (=coupling) and more proton leaks (=uncoupling).

To clarify the mechanism that underlies the increased uncoupling of respiration and ATP synthesis in skeletal muscles of PGC-1α transgenic mice, we measured expression of mRNAs for uncoupling protein UCP1, UCP2, and UCP3. UCP1 mRNA was not expressed in gastrocnemius from PGC-1α transgenic mice. In contrast, expression of UCP2 increased threefold, and that of UCP3 mRNA was decreased slightly (Figure 3C). In liver brown and white adipose tissues, there was no change in levels of UCP1, UCP2, and UCP3 mRNAs (data not shown). Although the role of UCP2 in uncoupling respiration has not been established,[30] the elevated expression of UCP2 might contribute, at least in part, to the uncoupling of respiration observed in PGC-1α transgenic mice.

We then measured the enzymatic activity of respiratory chain complex in mitochondria. Complex I, II, and III had similar activities in PGC-1α transgenic mice and wild-type mice; however, complex IV activity was increased twofold in the transgenic mice when expressed on a per citrate synthase activity basis (=mitochondrial number) (Table 2). An increase in levels of complex IV was confirmed by measurements of COX IV protein, a component of complex IV; COX IV levels in both PGC-1α transgenic mice lines were ~1.5-fold higher than those in wild-type mice, when expressed on a per citrate synthase activity basis (data not shown). Thus, the function of respiratory complexes was not impaired, but the ratio of the complexes was altered in PGC-1α transgenic mice.

ATP Content Was Markedly Decreased in PGC-1α Transgenic Mice

Because mitochondrial respiration in PGC-1α transgenic mice was attributable to proton leak rather than ATP synthesis, we hypothesized that PGC-1α transgenic mice would show reduced ATP levels in their skeletal muscle. To examine ATP levels, we measured the ATP and AMP contents of gastrocnemius (Figure 4). As expected, the ATP concentration in gastrocnemius from both lines of PGC-1α transgenic mice was ~80% lower than that in wild-type mice, whereas the AMP concentration was increased by fivefold to sevenfold. The alteration of the AMP/ATP ratio affects AMP-activated protein kinase (AMPK) activity.[31] Gastrocnemius from PGC-1α transgenic mice showed 4.7-fold higher α1 AMPK activity than control mice, whereas α2 AMPK activity was unchanged (data not shown), confirming that ATP depletion occurred *in vivo*.

PGC-1α Transgenic Mice Develop Skeletal Muscle Atrophy and Adipocyte Proliferation

A marked morphological change was observed in PGC-1α transgenic mice at 25 weeks of age compared with that of mice at 16 weeks of age (Figure 5, B and C). Quadriceps and gastrocnemius muscle (fastest and glycolytic type-2B fiber-rich muscle) from 25-week-old transgenic mice were paler in color than those of wild-type mice (Figure 5, A and C). This change was not observed in soleus muscle (type-1 fiber-rich muscle) (data not shown).

Histological analysis was performed to examine whether the pale, fat-like appearance of the gastrocnemius muscle in transgenic mice was attributable to increased lipid accumulation within myocytes or to an increased adipocyte numbers in skeletal muscles (Figure 5, D–I). Severe muscle atrophy was observed in PGC-1α transgenic mice, and myocytes were replaced by white

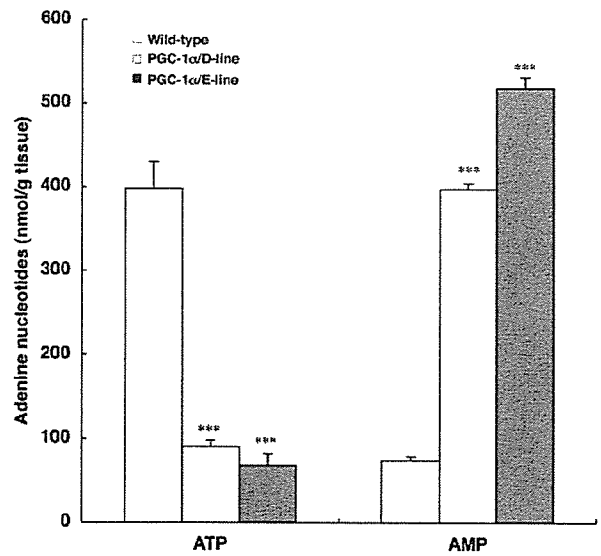

Figure 4. ATP content was markedly decreased in PGC-1α transgenic mice. ATP and AMP contents of gastrocnemius from wild-type, D-line, and E-line transgenic mice were measured at 10 weeks of age. Data are mean ± SEM values ($n = 3$). ***$P < 0.001$ versus wild-type mice.

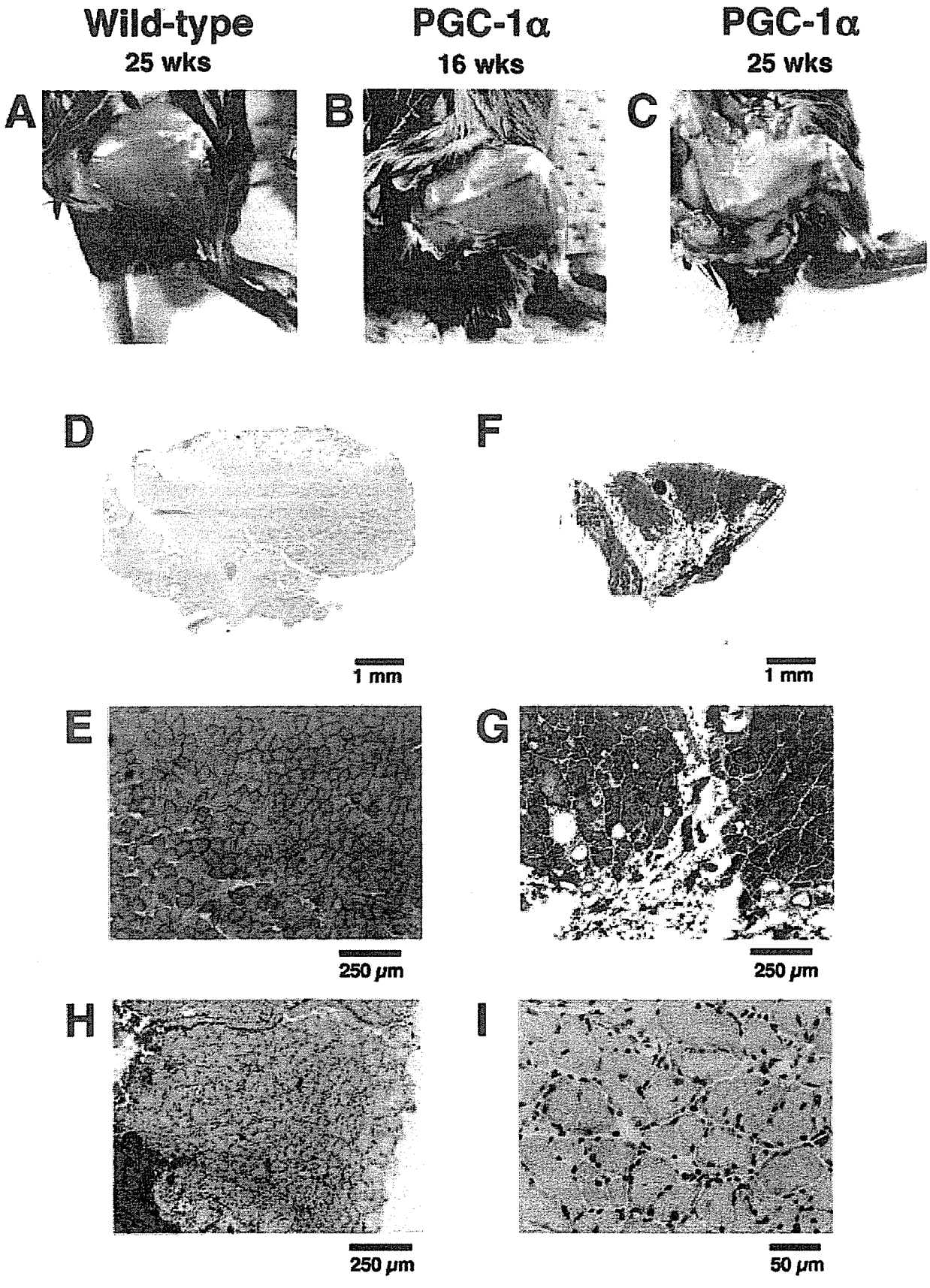
Wild-type
25 wks
PGC-1α
16 wks
PGC-1α
25 wks
A
B
C
D
F
1 mm
1 mm
E
G
250 μm
250 μm
H
I
250 μm
50 μm

Table 3. Physiological Characteristics of 25-Week-Old Wild-Type and PGC-1α Transgenic Male Mice

	Wild type (n = 4)	PGC-1α transgenic (D-line) (n = 3)	PGC-1α transgenic (E-line) (n = 4)
Body weight (g)	41.7 ± 0.6	32.0 ± 3.7*	30.7 ± 1.8†
Body fat (g)	10.4 ± 0.7	6.9 ± 1.1	6.9 ± 0.7*
Body fat (%)	30.4 ± 1.8	26.0 ± 3.7	26.0 ± 1.7
Lean body mass (g)	23.6 ± 0.8	19.4 ± 0.8†	19.5 ± 0.3†
Bone mineral density (g/cm^2)	0.051 ± 0.001	0.046 ± 0.000‡	0.043 ± 0.001‡
White adipose tissue weight (g)			
Epididymal	1.78 ± 0.15	0.88 ± 0.27†	0.66 ± 0.17‡
Retroperitoneal	0.46 ± 0.04	0.38 ± 0.12	0.31 ± 0.09
Subcutaneous	1.64 ± 0.15	0.93 ± 0.29	0.69 ± 0.14*
Brown adipose tissue weight (g)	0.28 ± 0.03	0.13 ± 0.01‡	0.11 ± 0.02‡
Gastrocnemius weight (g)	0.32 ± 0.01	0.17 ± 0.00‡	0.16 ± 0.00‡
Quadriceps weight (g)	0.34 ± 0.01	0.22 ± 0.05*	0.21 ± 0.01†
Liver weight (g)	1.70 ± 0.13	1.17 ± 0.09	1.30 ± 0.05
Spleen weight (g)	0.10 ± 0.00	0.06 ± 0.01	0.08 ± 0.01
Kidney weight (g)	0.48 ± 0.02	0.37 ± 0.02*	0.39 ± 0.01*
Heart weight (g)	0.17 ± 0.01	0.17 ± 0.01	0.17 ± 0.01
Food intake (g/g body weight/day)	0.156 ± 0.014	0.195 ± 0.017	0.192 ± 0.017

*$P < 0.05$, †$P < 0.01$, and ‡$P < 0.001$ versus wild-type mice.

adipose and connective tissues (Figure 5, F and G). Oil red O staining confirmed that the lipid accumulation was attributable not to myocytes but to adipocytes (Figure 5, H and I). Expression of mRNAs typically observed in adipose tissues, such as aP2, HSL, and perilipin, was significantly higher in gastrocnemius from PGC-1α transgenic mice than in gastrocnemius from wild-type mice at 25 weeks of age (data not shown). At 16 weeks of age, increases in the interstitial cell number and amount of connective tissue were observed, but lipid accumulation was absent (Figure 2). These data indicate that, in skeletal muscle tissues from PGC-1α transgenic mice, infiltration of adipocytes occurs rapidly from 4 to 6 months of age, concomitant with the progression of muscle atrophy.

PGC-1α Transgenic Mice Were 25% Smaller than Wild-Type Mice at 25 Weeks of Age

To further characterize PGC-1α transgenic mice, body composition and tissue weights were measured in two independent lines of PGC-1α transgenic mice at 25 weeks of age (Table 3). Although food intake was not different from controls, mean body weight of PGC-1α transgenic mice in both lines was ~25% lower than that of wild-type mice. DEXA scan revealed that both fat mass and lean body mass were decreased in transgenic mice. Bone mineral density was also significantly lower in PGC-1α transgenic mice. The tissue weights of white adipose tissue, brown adipose tissue, skeletal muscles, liver, spleen, and kidney in transgenic mice were 30 to 50% lower than those in wild-type mice. Thus, PGC-1α transgenic mice showed growth retardation with reductions in both lean body mass and fat mass.

Discussion

In the present study, we found that overexpression of PGC-1α in mouse skeletal muscle increased mitochondria numbers and energy expenditure, and eventually caused muscle atrophy, especially of type 2B fiber-rich muscles. PGC-1α transgenic mice showed normal mitochondrial COX and SDH activities (Figure 2, G and H) and normal respiratory chain enzymatic activities (Table 2); however, ATP content was reduced by increased uncoupling.

The marked decrease in the ATP content of type-2B fiber-rich muscles suggests that ATP depletion might be a major cause of muscle atrophy in PGC-1α transgenic mice (Figures 4 and 5). Consistent with our present findings, overexpression of PGC-1α in heart promotes mitochondrial biogenesis but leads to dilated cardiomyopathy.[4] ATP depletion due to impairment of mitochondrial functions is involved in the pathogenesis of a wide variety of inherited and acquired human diseases, including cardiomyopathy, neuromuscular dysfunction, and diabetes mellitus.[32] In skeletal muscles, inherited mitochondrial myopathy is due to mutations of genes encoding enzymes responsible for ATP synthesis in mitochondria.[28] Thus, their mitochondria show impaired mitochondrial respiratory function (=ATP synthesis). These mitochondria are increased in number and size and occasionally show abnormal structures, possibly as adaptation against decreased ATP content.[33] In acquired cases of muscle atrophy, aging-mediated muscle atrophy, namely sarcopenia, was mostly due to loss of type-2 fibers.[34,35] In sarcopenia, an increase in intramuscular adipose tissue was accompanied by a reduction in muscle fibers,[36]

Figure 5. Morphological and histological changes in skeletal muscles at 25 weeks of age. **A–C:** Lateral view of hindlimbs from wild-type (**A:** 25 weeks of age) and E-line transgenic (**B:** 16 weeks of age, **C:** 25 weeks of age) mice. Morphological differences were not observed in wild-type muscle between 16 and 25 weeks of age (data not shown). **D–G:** H&E staining of tissue sections from gastrocnemius of wild-type (**D**, **E**) and E-line transgenic mice (**F**, **G**). Specimens from transgenic mice showed atrophy of myocytes and increased adipose and interstitial connective tissues. **H** and **I:** Oil red O staining of tissue sections from gastrocnemius of E-line transgenic mice (**H**, **I**). Staining of lipid was observed in adipose tissue that surrounded the atrophic myocytes (**H**). No positive staining was observed inside the muscle fiber (**I**). Similar results were obtained for D-line transgenic mice (data not shown).

as was observed in our PGC-1α transgenic mice. *In vivo* proton magnetic resonance spectroscopy studies revealed that the mitochondrial ATP synthesis rate in skeletal muscle from elderly people was 46% lower than that in muscles from young patients.[37] Isolated mitochondria from elderly participants showed decreased state 3 (activated) mitochondrial respiration.[38] Taken together, these data indicate that ATP depletion caused by mitochondrial dysfunction might be a cause of sarcopenia. Therefore, ATP depletion in skeletal muscle might be a common feature of muscle atrophy.

However, reported clinical cases of ATP depletion attributable to increased uncoupling of respiration are very rare. Uncoupling-mediated muscle atrophy in humans was first described by Luft and colleagues[8,9] in 1959 and was called Luft's disease. This disease is important not only because it was the first identified human mitochondrial disorder but also because Luft's disease is still the only mitochondrial disease caused by uncoupling of oxidative phosphorylation. The cause of Luft disease is unknown because this disease is extremely rare; only one patient has been reported by DiMauro and colleagues[10] and in addition to the original case described by Luft and colleagues. To date, no animal model has been available. Patients with Luft's disease show increased energy expenditure and reduced body weight; however, thyroid hormone levels are normal. PGC-1α transgenic mice also exhibit these cardinal features with biochemical evidence of uncoupling of oxidative phosphorylation. Therefore, our mice recapitulate the phenotype of Luft's disease, although there is some difference in mitochondrial morphology. Mitochondria in Luft's disease were highly variable in size and shape with a range of abnormal internal structures, including densely packed cristae, tubular structures, electron-dense regularly layered cores, and concentric structures.[9,10,39] In PGC-1α transgenic mice, such morphological abnormalities in mitochondria were not observed. The reasons for these differences are unknown. The mechanism that underlies increased uncoupling of respiration by PGC-1α overexpression is also not clear. Increased expression of UCP2 may partially contribute to uncoupling (Figure 3C), but other unknown uncoupling proteins might also be involved.

The hypothesis that ATP depletion induces muscle atrophy may be supported by the fact that overexpression of UCP1 in skeletal muscle also reduces the masses of type-2B fiber-rich muscles (gastrocnemius and plantaris), which are vulnerable to ATP depletion, but not those of heart and soleus muscle, which undergo constant repeated contractions with high ATP supply.[40] Similar phenotype of mice overexpressing UCP1, the soleus muscle in PGC-1α transgenic mice is not atrophic, suggesting a close relation between ATP content and muscle mass. In fact, after exercise training, the number of functional mitochondria and glucose and fatty acid oxidation are increased in skeletal muscle, possibly because of an increase of PGC-1α; however, muscle weight is increased.[41] Thus, when myocyte energy expenditure is increased, a large supply of substrate from blood fatty acids and glucose might be required for maintenance of skeletal muscle integrity. Thus, mismatch between energy demand and supply may precipitate organ dysfunction.

Although the respiratory functions of complexes I, II, III, and IV in PGC-1α transgenic mice were not impaired, the activity of complex IV activity was much higher than those of complexes I, II, and III (Table 2). Conversely, in humans, a significant age-related decline in COX activity (complex IV of the respiratory chain) has been observed, but SDH activity (complex II of the respiratory chain) is not altered.[42] These data further indicate that aging might reduce PGC-1α activity in skeletal muscle. It is not clear why complex IV was preferentially activated by PGC-1α overexpression. Complexes I, II, and III are the significant sources of reactive oxygen species, namely superoxide and hydrogen peroxide, whereas complex IV is not.[43] We observed increased superoxide anion production in mitochondria from PGC-1α transgenic mice, when isolated mitochondria were incubated with either NADH (twofold increase per mg protein) or succinate (fourfold increase per mg protein) (data not shown). To prevent harmful increases in reactive oxygen species, adaptive mechanisms might suppress increases in expression of complexes I, II, and III in transgenic mice.

In this study, we demonstrated that overexpression of PGC-1α increased uncoupled oxidative phosphorylation and caused ATP deprivation, resulting in muscle atrophy, the phenotype of the first human mitochondrial disease described by Luft and colleagues,[8,9] more than 50 years ago. This mouse model confirms Luft's historical observation that uncoupling of oxidative phosphorylation causes myopathy. Furthermore, our results suggest that the genetic cause of Luft's disease may be a defect in the PGC-1α-related pathway. However, this is impossible to confirm until a new case can be found. Development of a mouse model of Luft's disease prompts further studies to understand the molecular mechanisms by which uncoupled oxidative phosphorylation leads to muscle atrophy.

Acknowledgments

We thank Dr. Ikuya Nonaka and Dr. Yu-ichi Goto at the National Center of Neurology and Psychiatry (Tokyo) for advice on mitochondrial myopathy and Dr. Constantine Londos at the National Institutes of Health (Bethesda, MD) for providing perilipin cDNA.

References

1. Puigserver P, Wu Z, Park CW, Graves R, Wright M, Spiegelman BM: A cold-inducible coactivator of nuclear receptors linked to adaptive thermogenesis. Cell 1998, 92:829–839
2. Wu Z, Puigserver P, Andersson U, Zhang C, Adelmant G, Mootha V, Troy A, Cinti S, Lowell B, Scarpulla RC, Spiegelman BM: Mechanisms controlling mitochondrial biogenesis and respiration through the thermogenic coactivator PGC-1. Cell 1999, 98:115–124
3. Vega RB, Huss JM, Kelly DP: The coactivator PGC-1 cooperates with peroxisome proliferator-activated receptor alpha in transcriptional control of nuclear genes encoding mitochondrial fatty acid oxidation enzymes. Mol Cell Biol 2000, 20:1868–1876
4. Lehman JJ, Barger PM, Kovacs A, Saffitz JE, Medeiros DM, Kelly DP: Peroxisome proliferator-activated receptor gamma coactivator-1 pro-

motes cardiac mitochondrial biogenesis. J Clin Invest 2000, 106:847–856
5. Lin J, Wu H, Tarr PT, Zhang CY, Wu Z, Boss O, Michael LF, Puigserver P, Isotani E, Olson EN, Lowell BB, Bassel-Duby R, Spiegelman BM: Transcriptional co-activator PGC-1 alpha drives the formation of slow-twitch muscle fibres. Nature 2002, 418:797–801
6. Miura S, Kai Y, Ono M, Ezaki O: Overexpression of peroxisome proliferator-activated receptor gamma coactivator-1alpha down-regulates GLUT4 mRNA in skeletal muscles. J Biol Chem 2003, 278:31385–31390
7. St.-Pierre J, Lin J, Krauss S, Tarr PT, Yang R, Newgard CB, Spiegelman BM: Bioenergetic analysis of peroxisome proliferator-activated receptor gamma coactivators 1alpha and 1beta (PGC-1alpha and PGC-1beta) in muscle cells. J Biol Chem 2003, 278:26597–26603
8. Ernster L, Ikkos D, Luft R: Enzymic activities of human skeletal muscle mitochondria: a tool in clinical metabolic research. Nature 1959, 184:1851–1854
9. Luft R, Ikkos D, Palmieri G, Ernster L, Afzelius B: A case of severe hypermetabolism of nonthyroid origin with a defect in the maintenance of mitochondrial respiratory control: a correlated clinical, biochemical, and morphological study. J Clin Invest 1962, 41:1776–1804
10. DiMauro S, Bonilla E, Lee CP, Schotland DL, Scarpa A, Conn Jr H, Chance B: Luft's disease. Further biochemical and ultrastructural studies of skeletal muscle in the second case. J Neurol Sci 1976, 27:217–232
11. Tsuboyama-Kasaoka N, Takahashi M, Tanemura K, Kim HJ, Tange T, Okuyama H, Kasai M, Ikemoto S, Ezaki O: Conjugated linoleic acid supplementation reduces adipose tissue by apoptosis and develops lipodystrophy in mice. Diabetes 2000, 49:1534–1542
12. Black JT, Judge D, Demers L, Gordon S: Ragged-red fibers. A biochemical and morphological study. J Neurol Sci 1975, 26:479–488
13. Seligman AM, Karnovsky MJ, Wasserkrug HL, Hanker JS: Nondroplet ultrastructural demonstration of cytochrome oxidase activity with a polymerizing osmiophilic reagent, diaminobenzidine (DAB). J Cell Biol 1968, 38:1–14
14. Dubowitz V, Brooke M: A Modern Approach, Muscle Biopsy. London, Saunders, 1973
15. Pallotti F, Lenaz G: Isolation and subfractionation of mitochondria from animal cells and tissue culture lines. Methods Cell Biol 2001, 65:1–35
16. Lowry OH, Rosebrough NJ, Farr AL, Randall RJ: Protein measurement with the Folin phenol reagent. J Biol Chem 1951, 193:265–275
17. Trounce IA, Kim YL, Jun AS, Wallace DC: Assessment of mitochondrial oxidative phosphorylation in patient muscle biopsies, lymphoblasts, and transmitochondrial cell lines. Methods Enzymol 1996, 264:484–509
18. Kita K, Vibat CR, Meinhardt S, Guest JR, Gennis RB: One-step purification from Escherichia coli of complex II (succinate: ubiquinone oxidoreductase) associated with succinate-reducible cytochrome b556. J Biol Chem 1989, 264:2672–2677
19. Miyadera H, Amino H, Hiraishi A, Taka H, Murayama K, Miyoshi H, Sakamoto K, Ishii N, Hekimi S, Kita K: Altered quinone biosynthesis in the long-lived clk-1 mutants of Caenorhabditis elegans. J Biol Chem 2001, 276:7713–7716
20. Ventura B, Genova ML, Bovina C, Formiggini G, Lenaz G: Control of oxidative phosphorylation by complex I in rat liver mitochondria: implications for aging. Biochim Biophys Acta 2002, 1553:249–260
21. Birch-Machin MA, Turnbull DM: Assaying mitochondrial respiratory complex activity in mitochondria isolated from human cells and tissues. Methods Cell Biol 2001, 65:97–117
22. Srere PA: Citrate synthase. Methods Enzymol 1969, 13:3–11
23. Tsuboyama-Kasaoka N, Tsunoda N, Maruyama K, Takahashi M, Kim H, Ikemoto S, Ezaki O: Up-regulation of uncoupling protein 3 (UCP3) mRNA by exercise training and down-regulation of UCP3 by denervation in skeletal muscles. Biochem Biophys Res Commun 1998, 247:498–503
24. Laborda J: 36B4 cDNA used as an estradiol-independent mRNA control is the cDNA for human acidic ribosomal phosphoprotein PO. Nucleic Acids Res 1991, 19:3998
25. Watanabe A, Tsuneishi E, Takimoto Y: Analysis of ATP and its breakdown products in beef by reversed-phase HPLC. J Food Sci 1989, 54:1169–1172
26. Scott MD, Baudendistel LJ, Dahms TE: Rapid separation of creatine, phosphocreatine and adenosine metabolites by ion-pair reversed-phase high-performance liquid chromatography in plasma and cardiac tissue. J Chromatogr 1992, 576:149–154
27. Nagy TR, Clair AL: Precision and accuracy of dual-energy X-ray absorptiometry for determining in vivo body composition of mice. Obes Res 2000, 8:392–398
28. Larsson NG, Clayton DA: Molecular genetic aspects of human mitochondrial disorders. Annu Rev Genet 1995, 29:151–178
29. Brand M: Mitochondria: A Practical Approach. Edited by G Brown, C Cooper Oxford University Press, 1995, pp 39–62
30. Esteves TC, Brand MD: The reactions catalysed by the mitochondrial uncoupling proteins UCP2 and UCP3. Biochim Biophys Acta 2005, 1709:35–44
31. Hardie DG, Carling D, Carlson M: The AMP-activated/SNF1 protein kinase subfamily: metabolic sensors of the eukaryotic cell? Annu Rev Biochem 1998, 67:821–855
32. Wallace DC: Mitochondrial diseases in man and mouse. Science 1999, 283:1482–1488
33. Heddi A, Lestienne P, Wallace DC, Stepien G: Mitochondrial DNA expression in mitochondrial myopathies and coordinated expression of nuclear genes involved in ATP production. J Biol Chem 1993, 268:12156–12163
34. Larsson L, Sjodin B, Karlsson J: Histochemical and biochemical changes in human skeletal muscle with age in sedentary males, age 22–65 years. Acta Physiol Scand 1978, 103:31–39
35. Tomonaga M: Histochemical and ultrastructural changes in senile human skeletal muscle. Am Geriatr Soc 1977, 25:125–131
36. Song MY, Ruts E, Kim J, Janumala I, Heymsfield S, Gallagher D: Sarcopenia and increased adipose tissue infiltration of muscle in elderly African American women. Am J Clin Nutr 2004, 79:874–880
37. Petersen KF, Befroy D, Dufour S, Dziura J, Ariyan C, Rothman DL, DiPietro L, Cline GW, Shulman GI: Mitochondrial dysfunction in the elderly: possible role in insulin resistance. Science 2003, 300:1140–1142
38. Trounce I, Byrne E, Marzuki S: Decline in skeletal muscle mitochondrial respiratory chain function: possible factor in ageing. Lancet 1989, 1:637–639
39. Sjostrand FS: Molecular pathology of Luft disease and structure and function of mitochondria. J Submicrosc Cytol Pathol 1999, 31:41–50
40. Couplan E, Gelly C, Goubern M, Fleury C, Quesson B, Silberberg M, Thiaudiere E, Mateo P, Lonchampt M, Levens N, De Montrion C, Ortmann S, Klaus S, Gonzalez-Barroso MD, Cassard-Doulcier AM, Ricquier D, Bigard AX, Diolez P, Bouillaud F: High level of uncoupling protein 1 expression in muscle of transgenic mice selectively affects muscles at rest and decreases their IIb fiber content. J Biol Chem 2002, 45:43079–43088
41. Holloszy JO, Kohrt WM, Hansen PA: The regulation of carbohydrate and fat metabolism during and after exercise. Front Biosci 1998, 3:D1011–D1027
42. Müller-Höcker J: Cytochrome c oxidase deficient fibres in the limb muscle and diaphragm of man without muscular disease: an aged-related alteration. J Neurol Sci 1990, 100:14–21
43. Jezek P, Hlavatá L: Mitochondria in homeostasis of reactive oxygen species in cell, tissue, and organism. Int J Biochem Cell Biol 2005, 37:2478–2503

Running title: *Entamoeba histolytica* genome

Structure and Content of the *Entamoeba histolytica* Genome

C. Graham Clark[1,*], U. Cecilia M. Alsmark[2], Margit Hofer[3], Yumiko Saito-Nakano[4], Vahab Ali[5], Sabrina Marion[6,#], Christian Weber[6], Chandrama Mukherjee[7], Iris Bruchhaus[8], Egbert Tannich[8], Matthias Leippe[9], Thomas Sicheritz-Ponten[10], Peter G. Foster[11], John Samuelson[12], Christophe J. Noël[2], Robert P. Hirt[2], T. Martin Embley[2], Carol A. Gilchrist[13], Barbara J. Mann[13], Upinder Singh[14], John P. Ackers[1], Sudha Bhattacharya[15], Alok Bhattacharya[16], Anuradha Lohia[7], Nancy Guillén[6], Michael Duchêne[3], Tomoyoshi Nozaki[5] and Neil Hall[17]

1: Department of Infectious and Tropical Diseases, London School of Hygiene and Tropical Medicine, London WC1E 7HT, UK
2: Division of Biology, Newcastle University, Newcastle NE1 7RU, UK.
3: Department of Specific Prophylaxis and Tropical Medicine, Center for Physiology and Pathophysiology, Medical University of Vienna, A-1090 Vienna, Austria
4: Department of Parasitology, National Institute of Infectious Diseases, Tokyo, Japan
5: Department of Parasitology, Gunma University Graduate School of Medicine, Maebashi, Japan
6: Institut Pasteur, Unité Biologie Cellulaire du Parasitisme and INSERM U786, F-75015 Paris, France
7: Department of Biochemistry, Bose Institute, Kolkata 700054, India
8: Bernhard Nocht Institute for Tropical Medicine, D-20359 Hamburg
9: Zoologisches Institut der Universität Kiel, D-24098 Kiel, Germany
10: Center for Biological Sequence Analysis, BioCentrum-DTU, Technical University of Denmark, DK-2800 Lyngby, Denmark
11: Department of Zoology, Natural History Museum, London, SW7 5BD, UK.
12: Department of Molecular and Cell Biology, Boston University Goldman School of Dental Medicine, Boston, MA 02118, USA
13: Department of Medicine,Division of Infectious Diseases, University of Virginia Health Sciences Center, Charlottesville, VA 22908, USA
14: Departments of Internal Medicine, Microbiology, and Immunology, Stanford University School of Medicine, Stanford, CA 94305, USA
15: School of Environmental Sciences, Jawaharlal Nehru University, New Delhi 110067, India
16: School of Life Sciences and Information Technology, Jawaharlal Nehru University, New Delhi 110067, India
17: The Institute for Genomic Research, Rockville, MD 20850, USA

*Corresponding Author
Current address: Cell Biology and Biophysics Program, European Molecular Biology Laboratory, 69117 Heidelberg, Germany

ABSTRACT

The intestinal parasite *Entamoeba histolytica* is one of the first protists for which a draft genome sequence has been published. Although the genome is still incomplete, it is unlikely that many genes are missing from the list of those already identified In this review we summarise the features of the genome as they are currently understood and provide previously unpublished analyses of many of the genes.

1. INTRODUCTION

Entamoeba histolytica is one of the most widespread and clinically important parasites, causing both serious intestinal (amoebic colitis) and extraintestinal (amoebic liver abscess) diseases throughout the world. A recent WHO estimate (WHO, 1998) places *E. histolytica* second after *Plasmodium falciparum* as causing the most deaths annually (70,000) among protistan parasites.

Recently a draft of the complete genome of *E. histolytica* was published (Loftus *et al.*, 2005) making it one of the first protist genomes to be sequenced. The *E. histolytica* genome project was initiated in 2000 with funding from the Wellcome Trust and the National Institute of Allergy and Infectious Diseases to the Wellcome Trust Sanger Institute and The Institute for Genomic Research (TIGR) in the UK and the USA, respectively. The publication describing the draft sequence concentrated on the expanded gene families, metabolism and the role of horizontal gene transfer in the evolution of *E. histolytica.* In this review we summarise the structure and content of the *E. histolytica* genome in comparison to other sequenced parasitic eukaryotes, provide a description of the current assembly and annotation, place the inferred gene content in the context of what is known about the biology of the organism, and discuss plans for completing the *E. histolytica* genome project and extending genome sequencing to other species of *Entamoeba.*

The fact that the genome sequence is still a draft has several important consequences. The first is that a few genes may be missing from the sequence data we have at present, although the number is likely to be small. For example, at least one gene (amoebapore B) is not present in the genome data despite it having been cloned, sequenced and the protein extensively characterised well before the start of the genome project. The second consequence is that the assembly contains a number of large duplicated regions that may be assembly artifacts, meaning that the number of gene copies is over-estimated in several cases. These problems cannot as yet be resolved but should be eventually as more data becomes available. Nevertheless, it is important to remember these issues when reading the rest of this article.

As the number of genes in *E. histolytica* runs into several thousands it is not possible to discuss all of them. However, we have generated a number of tables that identify many genes and link them to their entries in GenBank using the relevant protein identifier. Only a few tables are included in the text of this review, but the others are available on line as supplementary material - http://pathema.tigr.org/pathema/entamoeba_resources.shtml. The *E. histolytica* genome project data are being 'curated' at TIGR and it is on that site that the most current version of the assembled genome will be found. The 'Pathema' database will hold the data and the annotation (http://pathema.tigr.org/). The gene tables are also linked to the appropriate entry in the Pathema database and the links will be maintained as the genome structure is refined over time.

Reference is made throughout the text to other species of *Entamoeba* where data are available. *Entamoeba dispar* is the sister species to *E. histolytica* and infects humans without causing symptoms. *Entamoeba invadens* is a reptilian parasite that causes invasive disease, primarily in snakes and lizards, and is widely used as a model for *E. histolytica* in the study of encystation although the two species are not very closely related (Clark *et al.*, 2006b). Genome projects for both these species are underway at TIGR and it is anticipated that